Eur. Phys. J. A (2022) 58:28
https://doi.org/10.1140/epja/s10050-022-00677-y

THE EUROPEAN PHYSICAL JOURNAL A

Regular Article - Theoretical Physics

Occupation numbers and nuclear transition matrix elements for $0\nu\beta^-\beta^-$ decay within a mechanism involving neutrino mass

V. K. Nautiyal[1], R. Gautam[1], N. Das[2], R. Chandra[1,a], P. K. Raina[3], P. K. Rath[2]

[1] Department of Physics, Babasaheb Bhimrao Ambedkar University, Lucknow 226025, India
[2] Department of Physics, University of Lucknow, Lucknow 226007, India
[3] Department of Physics, Indian Institute of Technology, Ropar, Rupnagar 140001, India

Received: 23 July 2021 / Accepted: 3 February 2022 / Published online: 13 February 2022

Communicated by Michael Bender

Abstract By reproducing the experimentally available subshell occupation numbers of ^{100}Mo, ^{100}Ru, ^{128,130}Te, and ^{130}Xe nuclei, sets of four HFB intrinsic wave functions are generated with single particle energies due to Woods–Saxon potential and four different parametrizations of pairing plus multipolar effective two body interaction. In the rest of the considered nuclei, the single particle energies are scaled accordingly. Reliability of wave functions has been ascertained by comparing theoretically calculated and observed yrast spectra and deformation parameters β_2. Comparison between NTMEs $\overline{M}^{(K)}$ ($K = 0\nu$ and $0N$) calculated with wave functions having adjusted and unadjusted occupation numbers shows that the former are in general reduced. Uncertainties in set of twelve nuclear transition matrix elements for the neutrinoless double-β decay of ^{94,96}Zr, ^{100}Mo, ^{110}Pd, ^{128,130}Te, and ^{150}Nd isotopes calculated using three different parametrizations of Jastrow short range correlations turn out to be 10–14% and 37% due to the exchange of light and heavy Majorana neutrino, respectively.

1 Introduction

The neutrinoless double beta ($0\nu\beta\beta$) decay is one of the captivating processes in the scenario of lepton number violation as its experimental observation will prove the Majorana nature of massive neutrinos. The occurrence of $0\nu\beta\beta$ decay is possible within mechanisms of different gauge theoretical models involving left-right symmetry, R_p violating supersymmetry, sterile neutrinos, Majorons, leptoquarks, composite neutrinos, and extra-dimensional scenarios. The main objective of a large number of experimental projects is to observe the occurrence of $0\nu\beta\beta$ decay and using the available limits on half-lives $T^{(0\nu)}_{1/2}$ of $0\nu\beta\beta$ decay [1,2], stringent limits on gauge theoretical parameters have already been extracted in the theoretical studies [3,4]. In the reliable extraction of bounds on gauge theoretical parameters, the accuracy of model dependent nuclear transition matrix elements (NTMEs) plays a crucial role.

Within standard mass mechanism, the NTMEs have already been calculated in a number of nuclear models [5]. With the success of QRPA [6,7], its extension [8,9], and QRPA with isospin restoration [10] in explaining the observed quenching of double Gamow-Teller matrix elements, interacting shell-model (ISM) [11–23] has also been employed in this endeavor. In the evaluation of NTMEs, employment of ISM is the best option, if feasible. However, large-scale shell model calculations, although quite successful in explaining a large number of observed properties of nuclei [24,25], are constrained in the description of medium- and heavy-mass deformed nuclei due to limitations in the available computational capabilities.

Consideration of deformation degrees of freedom has been attempted in the deformed QRPA [26–29] with isospin restoration [30], projected-Hartree–Fock–Bogoliubov (PHFB) [31–34], the generator coordinate method (GCM) [35], beyond mean field covariant density functional theory (BMFCDFT) [36,37], and interacting boson model (IBM) [38–42] with isospin restoration [43]. In the calculation of NTMEs, several alternative uses of model space, single particle energies, effective two-body residual interactions, model dependent form factors to include the finite size of nucleons (FNS) [32], short range correlations (SRC) with Miller-Spencer parametrization [44], unitary operator method (UCOM) [45,46] parametrization based on coupled cluster method (CCM) [47], and the value of axial vector current coupling constant g_A [43,48–50] are available. Inter-

[a] e-mail: ramesh.luphy@gmail.com (corresponding author)

estingly, the calculated NTMEs $M^{(0\nu)}$ differ by factor of 2–3 in spite of the above mentioned several available alternatives.

In Refs. [32,33], NTMEs for $0\nu\beta^-\beta^-$ decay of ^{94,96}Zr, ^{100}Mo, ^{110}Pd, ^{128,130}Te, and ^{150}Nd isotopes have been calculated within standard mass mechanism using PHFB model. The HFB intrinsic wave functions were generated using a set of single particle energies (SPEs) that has been employed in a number of successful shell model [51] as well as variational-model calculations [52,53] and four different parametrizations of pairing plus multipolar effective two-body interaction. The strengths of pairing and quadrupole-quadrupole interactions were adjusted to reproduce the excitation energies E_{2^+} of 2^+ states. Over the past years, the experimental sub-shell occupation numbers of ^{100}Mo, ^{100}Ru, ^{128,130}Te, and ^{130}Xe nuclei have already been made available [54,55]. The reproduction of occupation numbers in addition to other available spectroscopic properties can play a crucial role in improving the reliability of model wave functions used in the calculation of NTMEs.

In the present work, we calculate NTMEs for the $0\nu\beta^-\beta^-$ decay of ^{94,96}Zr, ^{100}Mo, ^{110}Pd, ^{128,130}Te, and ^{150} Nd isotopes employing a set of four HFB intrinsic wave functions generated by using SPEs derived from Woods-Saxon potential [56] and four different parametrizations of pairing plus multipolar effective two-body interaction adjusted to reproduce the available experimental sub-shell occupation numbers. The present paper is organized as follows. The theoretical formalism to calculate the half-lives of the $0\nu\beta^-\beta^-$ decay is given in Sect. 2. In Sect. 3, we present the results and discuss them vis-a-vis the existing calculations done in other nuclear models. Finally, the conclusions are given in Sect. 4.

2 Theoretical formalism

The detailed theoretical formalism required for the study of $0\nu\beta^-\beta^-$ decay within the Majorana neutrino mass mechanism has been given in Refs. [57,58]. Within the PHFB approach, the calculation of NTMEs due to the exchange of light [32] and heavy Majorana [33] neutrinos has already been reported. In the following, we present a brief outline of the required formalism for clarity in notations used in the present paper.

Within Majorana neutrino mass mechanism, the half-life $T^{(0\nu)}_{1/2}$ for the $0^+ \to 0^+$ transition of $0\nu\beta^-\beta^-$ decay is given by

$$\left[T^{(0\nu)}_{1/2}(0^+ \to 0^+)\right]^{-1} = G_{01}\left|\frac{\langle m_\nu\rangle}{m_e}M^{(0\nu)} + \frac{m_p}{\langle M_N\rangle}M^{(0N)}\right|^2, \quad (1)$$

where

$$\langle m_\nu\rangle = \sum_i{}' U^2_{ei} m_i, \qquad m_i < 10\ \text{eV}, \quad (2)$$

$$\langle M_N\rangle^{-1} = \sum_i{}'' U^2_{ei} m_i^{-1}, \qquad m_i > 10\ \text{GeV}, \quad (3)$$

$$M^{(0K)} = -\frac{M^{(0K)}_F}{g_A^2} + M^{(0K)}_{GT} + M^{(0K)}_T, \quad (4)$$

and $K = 0\nu\ (0N)$ denotes mass mechanism due to the exchange of light (heavy) Majorana neutrinos. It is noteworthy that within seesaw model, the $0\nu\beta^-\beta^-$ decay has been studied by Blenow et al. [59] and Šimkovic et al. [60] and the conclusions need due attention. The phase space factors

$$G_{01} = \left[\frac{2\,(G_F g_A)^4\, m_e^9}{64\pi^5\,(m_e R)^2 \ln(2)}\right]\int_1^{T+1} f^{(0)}_{11}\, p_1 p_2 \varepsilon_1 \varepsilon_2 d\varepsilon_1 \quad (5)$$

have been recently calculated with good accuracy incorporating the screening correction [61–63] and within the PHFB model, the calculation of the NTMEs $M^{(K)}$ of the $0\nu\beta^-\beta^-$ decay in conjunction with their explicit structure has already been discussed in Refs. [31–33].

Employing HFB wave functions, one obtains the following expression for the NTME $M^{(K)}_\alpha$ of $0\nu\beta^-\beta^-$ decay corresponding to an operator $O^{(K)}_\alpha$ [31]:

$$\begin{aligned} M^{(K)}_\alpha &= \left\langle 0^+_f \middle\| O^{(K)}_\alpha \middle\| 0^+_i \right\rangle = \left[n^{Ji=0} n^{Jf=0}\right]^{-1/2} \\ &\times \int_0^\pi n_{(Z,N),(Z+2,N-2)}(\theta) \sum_{\alpha\beta\gamma\delta} \left\langle \alpha\beta \middle| O^{(K)}_\alpha \middle| \gamma\delta \right\rangle \\ &\times \sum_{\varepsilon\eta} \frac{\left(f^{(\pi)*}_{Z+2,N-2}\right)_{\varepsilon\beta}}{\left[\left(1 + F^{(\pi)}_{Z,N}(\theta) f^{(\pi)*}_{Z+2,N-2}\right)\right]_{\varepsilon\alpha}} \\ &\times \frac{\left(F^{(\nu)*}_{Z,N}\right)_{\eta\delta}}{\left[\left(1 + F^{(\nu)}_{Z,N}(\theta) f^{(\nu)*}_{Z+2,N-2}\right)\right]_{\gamma\eta}} sin\theta d\theta, \end{aligned} \quad (6)$$

where

$$\begin{aligned} n^J &= \int_0^\pi \left[det\left(1 + F^{(\pi)} f^{(\pi)^\dagger}\right)\right]^{1/2} \\ &\times \left[det\left(1 + F^{(\nu)} f^{(\nu)^\dagger}\right)\right]^{1/2} d^J_{00}(\theta) sin(\theta) d\theta. \end{aligned} \quad (7)$$

The required amplitudes (u_{im}, v_{im}) and expansion coefficients $C_{ij,m}$ of axially symmetric HFB intrinsic state $|\Phi_0\rangle$ with $K = 0$ for evaluating the expressions n^J, $n_{(Z,N),(Z+2,N-2)}(\theta)$, $f_{Z,N}$, and $F_{Z,N}(\theta)$ [31] are obtained by minimizing the expectation value of the effective Hamiltonian in a basis constructed by using a set of deformed states.

3 Results and discussions

In this work, the model space is same as used in Refs. [31–33]. Further, the Hamiltonian, which consists single particle part H_{sp} with pairing $V(P)$ plus quadrupole-quadrupole $V(QQ)$ (PQQ) plus hexadecapole-hexadecapole ($PQQHH$) parts of effective two-body interaction [32] is explicitly written as

$$H = H_{sp} + V(P) + V(QQ) + V(HH) \tag{8}$$

The single particle energies (SPEs) for ^{94,96}Zr, ^{94,96,100}Mo, ^{100}Ru, ^{110}Pd, ^{110}Cd, ^{128,130}Te, ^{128,130}Xe, ^{150} Nd, and ^{150}Sm isotopes are derived from Woods-Saxon potential as proposed by Blomqvist and Wahlborn [56] given by

$$\begin{aligned} V(r) = & -V_0 \frac{1}{1+\exp((r-R_0)/a)} \\ & -\lambda \left(\frac{\hbar}{2Mc}\right)^2 \mathbf{l}.\sigma \, \frac{1}{r}\frac{d}{dr}\left(\frac{V_0}{1+\exp((r-R_0)/a)}\right) \\ & +V_C(r) \end{aligned} \tag{9}$$

where $\lambda = 32.0$ is a dimensionless parameter, $a = 0.67$ is diffusitivity, and V_C is the Coulomb potential given as

$$V_C(r) = \begin{cases} Ze^2(3 - r^2/R_0^2)/2R_0 \ , & r \le R_0 \\ Ze^2/r & , r \ge R_0 \end{cases} \tag{10}$$

with $R_0 = r_0 A^{1/3}$ and $r_0 = 1.2$ fm. The potentials V_0 for protons and neutrons are taken as 57.0 MeV and 47.0 MeV, respectively. Using an effective two-body interaction consisting of pairing plus multipolar parts [64] with four different parametrizations, namely PQQ 1, $PQQHH1$, $PQQ2$, and $PQQHH2$ [31], four different sets of HFB intrinsic wave functions are generated.

The SPEs and strength of pairing and multipolar interactions are adjusted to reproduce the experimentally available sub-shell occupation numbers [54,55] and excitation energies E_{2^+} of 2^+ states of ^{100}Mo, ^{100}Ru, ^{128,130}Te, and ^{130}Xe isotopes. Specifically, the SPEs and strength of proton-neutron part of quadrupolar effective interaction are adjusted simultaneously with fixed pairing parameters to the desired end. In the present version of PHFB, the proton-neutron (pn) pairing has not been included. On the other hand, the importance of proton-neutron pairing has already been studied [6,65]. In Ref. [65], the PHFB calculation has been performed in a large model space in conjunction with pn-pairing and GCM. The deficiencies in present PHFB calculation needs to be removed and we intend to do so in future.

In Table 1, the adjusted occupation numbers due to $PQQ1$ parametrization (OC1) are given along with the unadjusted ones obtained from HFB wave functions (OC2) of Ref. [32] and experimentally observed data. The occupation numbers (η) calculated with other three parametrizations, namely $PQQHH1$, $PQQ2$, and $PQQHH2$ are found to be almost similar to those calculated with $PQQ1$ parametrization. Experimentally, both proton (only $0g_{9/2}$ orbit) and neutron occupation numbers of ^{100}Mo and ^{100}Ru isotopes have been reported. We denote the proton and neutron subshell occupation numbers by η_p and η_n, respectively. In case of ^{128,130}Te, and ^{130}Xe isotopes, experimental η_n are available. In comparison to our unadjusted η, the presently adjusted η are quite close to experimentally observed data but for η_p of ^{100}Mo and ^{100} Ru isotopes. In the rest of the nuclei, SPEs are scaled accordingly to reproduce excitation energies E_{2^+} of 2^+ states. The accuracy of reproduced excitation energies E_{2^+} is about 2%. In Table 2 , η_p and η_n due to OC1 and OC2 of ^{94,96}Zr, ^{94,96} Mo, ^{110}Pd, ^{110}Cd, ^{150}Nd, and ^{150}Sm isotopes for the $PQQ1$ parametrization are displayed. It is noticed that NTMEs $\overline{M}^{(K)}$ (Table 7) calculated with wave functions having adjusted experimental occupation numbers are in general reduced in comparison to those calculated without adjustment of the aforementioned experimental observable. The correlation between reduction in NTMEs $M^{(K)}$ with changing subshell occupation numbers η is discussed later.

Employing four sets of HFB intrinsic wave functions, the deformation parameters β_2 of the above mentioned nuclei are calculated for effective charges $e_{eff} = 0.40$, 0.50, and 0.60. In Table 3, the calculated averages and experimentally observed β_2 are presented. In all four parametrizations, the observed β_2 values of ^{96}Mo, ^{100}Ru, and ^{150}Sm are in overall agreement with calculated values with $e_{eff} = 0.40$. In case of ^{94}Zr but for the $PQQ2$ parametrization, ^{96}Zr, ^{110}Pd, ^{110}Cd, ^{130}Te, ^{128,130} Xe, ^{150}Nd isotopes the observed β_2 values are in good agreement with calculated values for $e_{eff} = 0.50$. In case of ^{94,100} Mo and ^{128}Te isotopes, the calculated values agree with experimental data with $e_{eff} = 0.60$. An *ab initio* perturbative calculation of effective charges [66] is based on Brandow's linked cluster expansion [67] in conjunction with folded diagram expansion due to Kuo [68]. In principle, the values of effective charges are dependent on the size of the model space and vary for different orbits and nucleon type. However, a very rough estimate of proton and neutron effective charges is given by $e_{eff} = Ze/A$ [69], which turns out to be 0.4–0.45 for the nuclei considered in the present work. Hence, the effective charges required to reproduce the experimental β_2 values are quite reasonable.

As shown in a number of QRPA [6,70,71] and ISM calculations [72–75], the closure approximation is not valid to calculate NTMEs $M_{2\nu}$ of $2\nu\beta^-\beta^-$ decay. However, the quality of wave functions is ascertained presently by estimating the average NTMEs $\overline{M}_{2\nu}$ (average of NTMEs $M_{2\nu}$ due to four sets of HFB intrinsic wave functions) presented in Table 4 for the $0^+ \rightarrow 0^+$ transition of $2\nu\beta^-\beta^-$ decay in closure approximation and comparing them with the available experimental data [76]. Neglecting Fermi matrix element $M_F^{(2\nu)}$,

Table 1 Adjusted occupation numbers (OC1) and experimental [54,55] ones of protons and neutrons for ^{100}Mo, ^{100}Ru, ^{128,130}Te, and ^{128,130}Xe isotopes with $PQQ1$ parametrization. The unadjusted occupation numbers (OC2) obtained from HFB wave functions of Ref. [32] are given in parenthesis

Nuclei		$2s_{1/2}$	$1p_{1/2}$	$1d$	$0g_{7/2}$	$0g_{9/2}$	$0h_{11/2}$
	Protons						
^{100}Mo		0.03 (0.04)	0.01 (0.11)	0.54 (0.51)	0.02 (0.02)	3.38 (3.28)	0.01(0.04)
	Exp.	–	–	–	–	4.06 ± 0.30	–
^{100}Ru		0.08 (0.04)	0.04 (1.04)	0.86 (0.48)	0.10 (0.04)	4.97 (4.33)	− 0.06 (0.69)
	Exp.	–	–	–	–	5.56 ± 0.22	–
	Neutrons						
^{100}Mo		0.31 (0.71)	1.99 (1.99)	3.68 (4. 53)	2.56 (1.42)	9.67 (9.84)	1.80 (1.51)
	Exp.	0.33 ± 0.02	–	3.40 ± 0.17	2.48 ± 0.19	–	1.89 ± 0.13
^{100}Ru		0.53 (0.63)	1.99 (2.00)	2.81 (4. 23)	2.34 (0.99)	9.11 (9.88)	1.21 (0.27)
	Exp.	0.23±0.01	–	2.50 ± 0.12	2.19±0.15	–	1.13 ± 0.08
		$2s_{1/2}$	$1d$	$1f_{7/2}$	$0g_{7/2}$	$0h_{9/2}$	$0h_{11/2}$
	Protons						
^{128}Te		0.38 (0.55)	1.56 (1. 37)	0.00 (0.00)	0.05 (0.09)	0.00 (0.00)	0.00 (0.00)
^{128}Xe		0.49 (0.59)	2.60 (2. 49)	0.01 (0.02)	0.89 (0.82)	0.00 (0.00)	0.00 (0.09)
^{130}Te		0.38 (0.48)	1.55 (1. 49)	0.00 (0.00)	0.06 (0.03)	0.00 (0.00)	0.00 (0.00)
^{130}Xe		0.46 (0.55)	2.77 (2. 86)	0.01 (0.00)	0.79 (0.52)	0.00 (0.00)	− 0.04 (0.06)
	Neutrons						
^{128}Te		1.33 (1.93)	7.97 (9. 67)	0.26 (0.65)	7.63 (6.80)	0.20 (0.22)	8.60 (6.73)
	Exp.	1.28 ± 0.2	7.94 ± 0.2	–	8.00	–	8.66 ± 0.3
^{128}Xe		1.61 (1.71)	8.57(8. 76)	1.37 (1.17)	6.18 (5.64)	0.38 (0.41)	5.89 (6.31)
^{130}Te		1.52 (1.97)	8.63 (9. 87)	0.21 (0.42)	7.71 (7.60)	0.14 (0.19)	9.80 (7.96)
	Exp.	1.50 ± 0.2	8.55 ± 0.2	–	8.00	–	9.79 ± 0.3
^{130}Xe		1.25 (1.92)	7.35 (9. 63)	0.54 (0.82)	7.49 (6.58)	0.40 (0.24)	8.96 (6.80)
	Exp.	1.44 ± 0.2	7.29 ± 0.2	–	8.00	–	9.01 ± 0.3

the NTME $M_{2\nu}$ in closure approximation is written as

$$M_{2\nu} = \frac{\left\langle 0_f^+ \left\| \sum_{n,m} \sigma_n \cdot \sigma_m \tau_n^+ \tau_m^+ \right\| 0_i^+ \right\rangle}{\langle E_N \rangle - (M_I + M_F)/2} = \frac{M_{GT}^{(2\nu)}}{E_d} \tag{11}$$

where the energy denominator $E_d = 1.12A^{1/2}$ MeV [77]. The experimental $M_{2\nu}$ are not available for ^{94}Zr and ^{110}Pd isotopes. The maximum uncertainty $\Delta\overline{M}_{2\nu}$ turns out to be about 21%, which shows that the NTMEs $M_{2\nu}$ are highly sensitive to the structure aspects of the intrinsic wave functions. The extracted g_{eff} are given along with those obtained in IBM [38–41] in the last two columns of the same Table 4.

Employing four sets of PHFB wave functions generated with four different parametrizations of pairing plus multipolar effective two-body interaction and three different parametrizations of the Jastrow type of SRC, namely SRC1, SRC2, and SRC3 [31], sets of twelve NTMEs $M^{(0\nu)}$ and $M^{(0N)}$ due to light and heavy Majorana neutrino exchange, respectively, are calculated for ^{94,96}Zr, ^{100} Mo, ^{110}Pd, ^{128,130}Te, and ^{150}Nd isotopes. In Table 5 , the calculated NTMEs $M^{(K)}(K = 0\nu$ and $0N)$ due to different approximations are presented. Further, the NTMEs $M^{(0\nu)}$ and $M^{(0N)}$ are calculated for point nucleons (P), nucleons with finite size (FNS), and with the consideration of FNS and SRC simultaneously (F+SRC) for all four parametrizations. The validity of closure approximation for $M^{(0\nu)}$ has been ascertained by calculating them in the case of F+SRC with $\overline{A}/2$ in the energy denominator.

It is noticed that in general, the NTMEs evaluated for both $PQQ1$ and $PQQ2$ parametrizations but for ^{110}Pd isotope are quite close. The inclusion of hexadecapolar term tends to reduce them by magnitudes, specifically depending on the structure of nuclei. The maximum variation in $M^{(0\nu)}$ due to the $PQQHH1$, $PQQ2$, and $PQQHH2$ parametrizations with respect to $PQQ1$ for all nuclei except ^{110}Pd is about 12%. However, the maximum variation in case of ^{110}Pd is about 37%. The relative change in NTMEs $M^{(0\nu)}$, by changing the energy denominator to $\overline{A}/2$ instead of $\overline{A}$ is in between 7.5–

Table 2 Adjusted occupation numbers (OC1) of protons and neutrons for ^{94,96}Zr, ^{94,96}Mo, ^{110}Pd, ^{110}Cd, ^{150}Nd, and ^{150}Sm isotopes with *PQQ*1 parametrization. The unadjusted occupation numbers (OC2) obtained from HFB wave functions of Ref. [32] are given in parenthesis

Nuclei	$2s_{1/2}$	$1p_{1/2}$	$1d$	$0g_{7/2}$	$0g_{9/2}$	$0h_{11/2}$
Protons						
^{94}Zr	0.01 (0.01)	0.14 (0.32)	0.18 (0.09)	0.01 (0.17)	1.61 (1.50)	0.04 (0.59)
^{94}Mo	0.02 (0.29)	0.58 (0.43)	0.31 (0.33)	0.02 (0.03)	2.99 (3.10)	0.08 (0.83)
^{96}Zr	0.01 (0.01)	0.81 (0.63)	0.04 (0.37)	0.01 (0.02)	1.07 (1.21)	0.06 (0.86)
^{96}Mo	0.03 (0.46)	0.13 (0.12)	0.51 (0.72)	0.02 (0.23)	3.32 (3.23)	− 0.02 (0.06)
^{110}Pd	0.14 (0.04)	1.73 (1.96)	1.05 (0.53)	0.15 (0.03)	4.96 (5.41)	− 0.04 (0.03)
^{110}Cd	0.01 (0.13)	2.00 (1.96)	0.43 (0.68)	0.03 (0.06)	7.52 (7.08)	0.00 (0.08)
Neutrons						
^{94}Zr	0.42 (0.47)	2.00 (1.99)	3.38 (3.20)	0.19 (0.16)	9.90 (9.92)	0.11 (0.25)
^{94}Mo	0.44 (0.61)	2.00 (2.00)	1.68 (1.51)	0.11 (0.74)	9.76 (9.80)	0.00 (0.00)
^{96}Zr	0.41 (0.67)	1.99 (1.98)	4.68 (4.42)	0.63 (0.43)	9.84 (9.89)	0.45 (0.60)
^{96}Mo	0.48 (0.64)	1.99 (2.00)	3.40 (2.82)	0.69 (0.64)	9.36 (9.72)	0.07 (0.19)
^{110}Pd	0.83 (1.01)	1.99 (1.99)	5.22 (5.86)	3.97 (2.79)	9.70 (9.89)	4.28 (4.45)
^{110}Cd	0.71 (0.90)	1.99 (1.99)	5.35 (5.46)	3.60 (2.28)	9.83 (9.88)	2.51 (3.49)
	$2s_{1/2}$	$1d$	$1f_{7/2}$	$0g_{7/2}$	$0h_{9/2}$	$0h_{11/2}$
Protons						
^{150}Nd	0.50 (0.58)	4.01 (4.27)	0.72 (0.70)	1.49 (1.15)	0.02 (0.02)	3.25 (3.29)
^{150}Sm	0.48 (0.70)	4.27 (5.37)	0.40 (0.50)	2.69 (1.87)	0.04 (0.04)	4.12 (3.52)
Neutrons						
^{150}Nd	1.99 (2.00)	9.97 (9.98)	4.19 (4.09)	7.94 (7.96)	5.92 (5.74)	9.98 (10.23)
^{150}Sm	1.99 (1.99)	9.96 (9.96)	2.20 (2.99)	7.97 (7.92)	5.07 (4.32)	10.80 (10.83)

Table 3 Theoretically calculated β_2 values of ^{94,96}Zr, ^{94,96,100}Mo, ^{100}Ru, ^{110}Pd, ^{110}Cd, ^{128,130}Te, ^{128,130} Xe, ^{150}Nd, and ^{150}Sm nuclei along with their experimental values. In the calculation of β_2, effective charge $e_{eff} = 0.40$ has been used for ^{96}Mo, ^{100}Ru, and ^{150}Sm isotopes. Similarly, $e_{eff} = 0.50$ for ^{94}Zr, ^{96}Zr, ^{110}Pd, ^{110}Cd, ^{130}Te, ^{128,130}Xe, ^{150}Nd isotopes as well as $e_{eff} = 0.60$ for ^{94,100}Mo and ^{128}Te isotopes have been used

Nuclei	β_2		Nuclei	β_2	
	Theo.	Exp. [78,79]		Theo.	Exp. [78,79]
^{94}Zr	0.0996 ± 0.0316	0.090 ± 0.010	^{94}Mo	0.1600 ± 0.0010	0.1509 ± 0.0015
^{96}Zr	0.0840±0.0020	0.080±0.017	^{96}Mo	0.1749 ± 0.0019	0.1720 ± 0.0016
^{100}Mo	0.2452±0.0005	0.2309±0.0022	^{100}Ru	0.2206 ± 0.0027	0.2148 ± 0.0011
^{110}Pd	0.2453±0.0092	0.257±0.006	^{110}Cd	0.1848 ± 0.0065	0.1770 ± 0.0039
^{128}Te	0.1389±0.0011	0.1363±0.0011	^{128}Xe	0.1838 ± 0.0022	0.1836 ± 0.0049
^{130}Te	0.1106±0.0065	0.1184±0.0014	^{130}Xe	0.1686 ± 0.0061	0.169 ± 0.007
^{150}Nd	0.2811±0.0009	0.2853±0.0021	^{150}Sm	0.2240 ± 0.0036	0.1931 ± 0.0021

12.4%, which confirms that the dependence of NTMEs on average excitation energy $\overline{A}$ is small and thus, the validity of the closure approximation for $0\nu\beta^-\beta^-$ decay is supported. In the case of NTMEs $M^{(0N)}$ due to heavy Majorana neutrino exchange, the effect due to different parametrizations is found to be similar as in case of NTMEs $M^{(0\nu)}$ due to light neutrino exchange.

The effects due to FNS and SRC are quantified as relative changes, the range of which corresponds to the minimum and maximum changes in sets of 28 (7 nuclei and 4 parametrizations) NTMEs $M^{(K)}(K = 0\nu, 0N)$. It is noticed that the consideration of FNS induces changes about 9.0–12.0% in the NTMEs $M^{(0\nu)}$ with respect to point nucleon case. Here, the range of relative changes corresponds to the minimum and maximum changes in sets of 28 (7 nuclei and 4 parametriza-

Table 4 Theoretically estimated average NTMEs $\overline{M}_{2\nu}$ within closure approximation along with experimental values [76]

Nucleus	$M_{2\nu}$(Exp.)	$\overline{M}_{2\nu}$		g_{eff}	
		PHFB	IBM [38–41]	PHFB	IBM [38–41]
^{94}Zr		0.091 ± 0.019			
^{96}Zr	0.080 ± 0.004	0.068 ± 0.002	0.10	1.08	0.89
^{100}Mo	0.185 ± 0.005	0.159 ± 0.006	0.13	1.08	1.19
^{110}Pd		0.138 ± 0.019	0.13		
^{128}Te	0.043 ± 0.003	0.052 ± 0.008	0.15	0.91	0.54
^{130}Te	0.0293 ± 0.0009	0.096 ± 0.007	0.13	0.55	0.48
^{150}Nd	0.055 ± 0.003	0.047 ± 0.004	0.06	1.08	0.96

Table 5 Calculated NTMEs $M^{(0\nu)}$ and $M^{(0N)}$ with (a) $PQQ1$, (b) $PQQHH1$, (c) $PQQ2$ and (d) $PQQHH$ 2 parametrizations for the $0\nu\beta^-\beta^-$decay of ^{94,96} Zr, ^{100}Mo, ^{104}Ru, ^{110}Pd, ^{128,130}Te, ^{150}Nd isotopes due to the exchange of light and heavy Majorana neutrinos, respectively

Nuclei		$M^{(0\nu)}$				$M^{(0N)}$			
		FNS	F+SRC			FNS	F+SRC		
			SRC1	SRC2	SRC3		SRC1	SRC2	SRC3
^{94}Zr	(a)	3.725	3.187	3.662	3.817	203.28	67.87	119.64	164.77
	(b)	3.423	2.921	3.364	3.509	189.58	63.29	111.56	153.65
	(c)	4.045	3.536	3.995	4.142	200.74	71.55	121.60	164.60
	(d)	3.312	2.822	3.254	3.395	184.42	61.23	108.27	149.33
^{96}Zr	(a)	2.581	2.192	2.534	2.645	141.90	44.94	81.81	114.12
	(b)	2.526	2.128	2.476	2.590	145.35	46.18	83.86	116.92
	(c)	2.514	2.134	2.468	2.577	138.55	43.76	79.78	111.38
	(d)	2.463	2.074	2.414	2.526	141.63	44.87	81.63	113.89
^{100}Mo	(a)	5.803	5.013	5.723	5.950	293.29	94.43	170.57	236.79
	(b)	5.480	4.717	5.402	5.621	284.82	92.77	166.37	230.32
	(c)	5.783	4.994	5.703	5.930	292.48	93.88	169.90	236.03
	(d)	5.399	4.641	5.321	5.538	282.25	91.60	164.64	228.12
^{104}Ru	(a)	3.185	2.666	3.151	3.300	203.81	70.51	122.70	166.98
	(b)	2.977	2.480	2.942	3.085	195.11	67.81	117.61	159.91
	(c)	3.298	2.765	3.262	3.415	209.06	72.10	125.68	171.18
	(d)	3.019	2.517	2.984	3.128	197.08	68.40	118.73	161.49
^{110}Pd	(a)	3.892	3.361	3.844	3.996	198.28	63.91	115.64	160.34
	(b)	5.335	4.624	5.269	5.473	270.90	90.77	160.34	220.26
	(c)	5.091	4.405	5.030	5.227	257.94	83.83	150.93	208.85
	(d)	4.710	4.067	4.651	4.835	244.13	81.31	144.15	198.32
^{128}Te	(a)	2.895	2.482	2.854	2.973	160.81	55.24	96.11	131.24
	(b)	2.633	2.221	2.590	2.708	159.62	54.74	95.31	130.21
	(c)	2.961	2.542	2.920	3.040	163.37	56.17	97.68	133.34
	(d)	2.604	2.190	2.561	2.680	160.54	55.10	95.89	130.98
^{130}Te	(a)	4.343	3.777	4.282	4.445	222.31	77.71	133.56	181.70
	(b)	3.974	3.421	3.911	4.070	216.98	76.03	130.35	177.29
	(c)	3.957	3.427	3.899	4.052	207.39	71.92	124.17	169.28
	(d)	4.341	3.758	4.276	4.444	229.74	81.08	138.49	187.99
^{150}Nd	(a)	2.544	2.219	2.516	2.610	128.22	44.00	76.74	104.74
	(b)	2.293	1.991	2.266	2.353	118.74	40.55	70.89	96.89
	(c)	2.825	2.463	2.794	2.899	143.18	49.14	85.71	116.97
	(d)	2.278	1.975	2.251	2.338	118.80	40.54	70.91	96.93

Table 6 Deformation ratios $D^{(0K)}$ for $0\nu\beta^-\beta^-$ decay of ^{94,96}Zr, ^{100}Mo, ^{110}Pd, ^{128,130}Te, and ^{150} Nd isotopes with *PQQ*1 parametrization

Nuclei	$D^{(0\nu)}$ F+SRC			$D^{(0N)}$ F+SRC		
	SRC1	SRC2	SRC3	SRC1	SRC2	SRC3
^{94}Zr	2.40	2.37	2.36	2.20	2.19	2.19
^{96}Zr	4.55	4.47	4.44	4.35	4.16	4.08
^{100}Mo	3.51	3.47	3.46	3.58	3.43	3.37
^{110}Pd	5.61	5.51	5.48	5.53	5.24	5.12
^{128}Te	3.14	3.09	3.08	2.78	2.77	2.75
^{130}Te	3.92	3.81	3.78	3.11	3.04	3.01
^{150}Nd	8.71	8.70	8.70	8.72	8.69	8.68

Table 7 Average NTMEs $\overline{M}^{(K)}$ ($K = 0\nu, 0N$) and uncertainties $\Delta\overline{M}^{(K)}$ for the $0\nu\beta^-\beta^-$ decay of ^{94,96}Zr, ^{100}Mo, ^{110}Pd, ^{128,130}Te, and ^{150}Nd isotopes along with those calculated in Refs. [32,33]

Nuclei	$\overline{M}^{(0\nu)}$		$\overline{M}^{(0N)}$	
	Ref. [32]	Present	Ref. [33]	Present
^{94}Zr	3.853 ± 0.371	3.467 ± 0.399	125.523 ± 44.576	113.11 ± 39.73
^{96}Zr	2.842±0.263	2.396±0.206	99.949±36.579	80.26 ± 29.54
^{100}Mo	6.216±0.633	5.379±0.448	205.618±72.474	164.62 ± 59.66
^{110}Pd	7.112±0.748	4.565±0.648	230.204±81.810	139.89 ± 53.05
^{128}Te	3.591±0.393	2.647±0.273	126.125±45.962	94.33 ± 32.51
^{130}Te	4.023±0.494	3.980±0.350	135.652±46.528	129.13 ± 44.04
^{150}Nd	2.810±0.427	2.390±0.285	85.086±31.196	74.50 ± 26.56

tions) NTMEs. Relative to the FNS case, the NTMEs $M^{(0\nu)}$ are further reduced by approximately 13.0–17.0%, 1.0–2.0%, and 2–3.0% with the addition of SRC1, SRC2, and SRC3, respectively. In case of heavy Majorana neutrino exchange, the change in $M^{(0N)}$ is about 29–33% due to the FNS with respect to the point nucleon case. With the inclusion of both FNS and SRC, the NTMEs are reduced by about 65–68%, 39–42%, and 18–20% for F+SRC1, F+SRC2, and F+SRC3, respectively.

The role of deformation in the calculation of $M^{(K)}$ has been ascertained by the quantity $D^{(K)}$ defined as the ratio of $M^{(K)}$ at zero deformation ($\zeta_{qq} = 0$) and full deformation ($\zeta_{qq} = 1$) [80].

$$D^{(K)} = \frac{M^{(K)}(\zeta_{qq} = 0)}{M^{(K)}(\zeta_{qq} = 1)}, \tag{12}$$

It may be mentioned that $M^{(K)}$ ($\zeta_{qq} = 0$) are calculated with wave functions generated neglecting proton-neutron quadrupolar interaction. The wave functions so generated are not realistic and the nuclear properties given in Tables 1, 2 and 3, cannot be reproduced. Hence, the ratios $D^{(K)}$ may be treated as estimates of upper limits on deformation effects. Owing to deformation effects (Table 6), the NTMEs $M^{(K)}$ of $0\nu\beta^-\beta^-$ decay are suppressed by a factor of about 2–9 in the mass range $A = 94 - 150$, the smallest and largest values of $D^{(K)}$ correspond to ^{94}Zr and ^{150}Nd nuclei, respectively. Thus, the deformation plays a crucial role in the nuclear structure aspects of $\beta^-\beta^-$ decay.

Employing set of twelve NTMEs (3 SRCs and 4 parametrizations), the uncertainties $\Delta\overline{M}^{(0\nu)}$ and $\Delta\overline{M}^{(0N)}$ associated with average NTMEs $\overline{M}^{(0\nu)}$ and $\overline{M}^{(0N)}$, respectively, are estimated by preforming a statistical analysis and are presented in Table 7. It turns out that the uncertainties $\Delta\overline{M}^{(0\nu)}$ are of the order of 10%, but for ^{110}Pd for which $\Delta\overline{M}^{(0\nu)}$ is approximately 14%. For the case of NTMEs associated with heavy Majorana neutrino exchange, the maximum uncertainty $\Delta\overline{M}^{(0N)}$ is about 37%. In the same Table 7, NTMEs $\overline{M}^{(0\nu)}$ and $\overline{M}^{(0N)}$ calculated with HFB wave functions without adjusting to experimental occupation numbers [32,33] and rescaled with $g_A = 1.2701$ [81] are also given in 1st and 3rd columns, respectively, for comparison. It is noticed that the calculated NTMEs $\overline{M}^{(0\nu)}$ and $\overline{M}^{(0N)}$ with wave functions due to adjustment of experimental occupation numbers are reduced by about 1–36% and 5–39%, respectively, in comparison to those calculated without adjustment of the aforementioned experimental observable. The smallest and largest reductions correspond to ^{130}Te and ^{110}Pd isotopes, respectively.

Before correlating the change in occupation numbers η between OC1 and OC2 with reduction in NTMEs $\overline{M}^{(K)}$, it may be mentioned that the former, given in Tables 1 and 2, are due to *PQQ1* parametrization and the latter

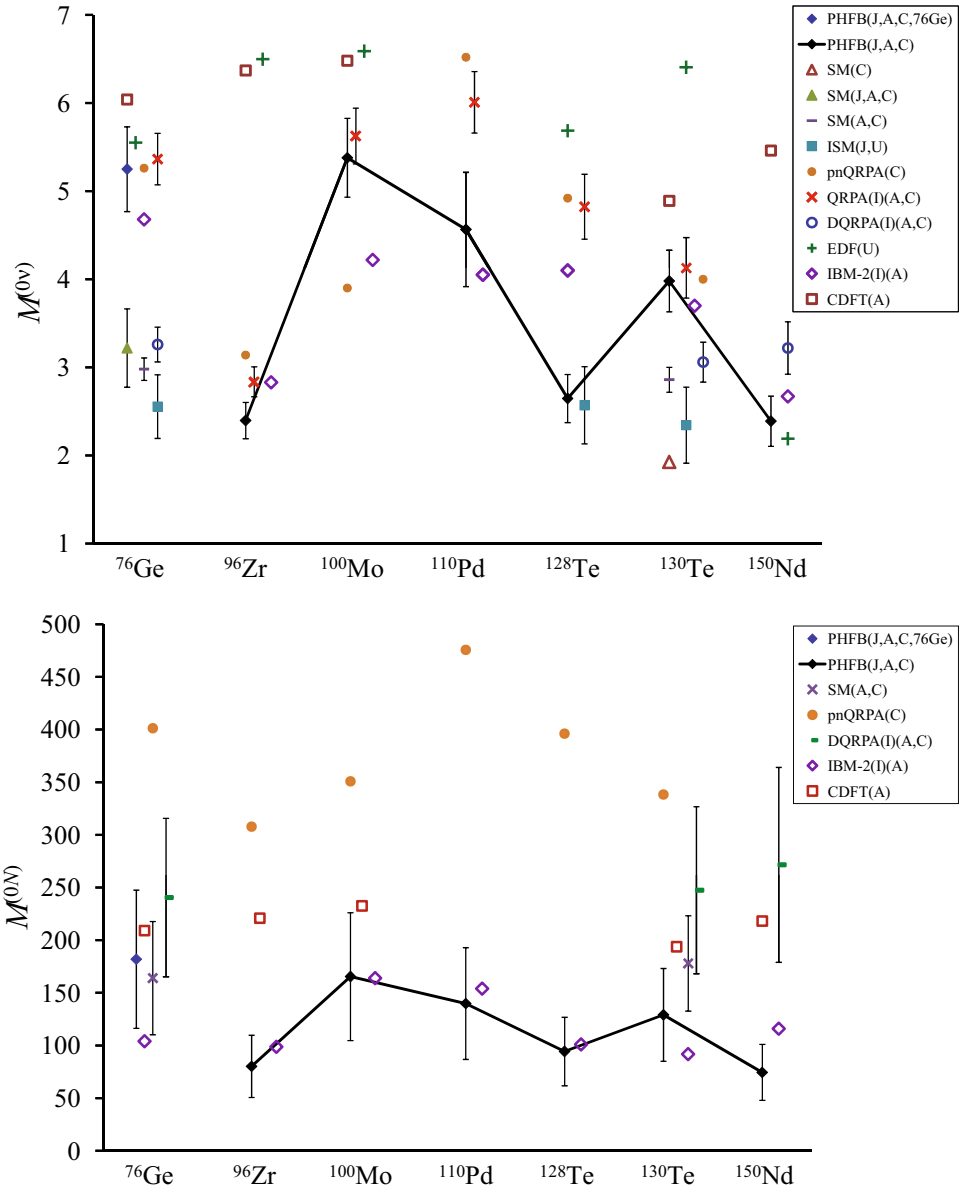

Fig. 1 NTMEs $M^{(0\nu)}$ and $M^{(0N)}$ calculated in SM [82–84], ISM [15], pnQRPA [85], QRPA(I) [10], DQRPA(I) [30], EDF [86], IBM-2(I) [43], and CDFT [37] models along with present work. The PHFB values of NTMEs for ^{76}Ge have been taken from Ref. [87]. J, A, C, and U represent the SRCs due to Jastrow, AV18, CD Bonn and UCOM parametrizations

are averages of NTMEs due to $PQQ1$, $PQQHH1$, $PQQ2$, and $PQQHH2$ parametrizations. However, η calculated with $PQQ1$ parametrizations are almost similar to those calculated with other three parametrizations. Further, η is the weighted sum of of v_{im}^2 and in the calculation of $M^{(0\nu)}$, the occupation and non-occupation probability amplitudes $v_{im}^{(i)}(n)u_{im}^{(i)}(p)$ and $v_{im}^{(f)}(p)u_{im}^{(f)}(n)$ are relevant. Hence, the reduction in $\overline{M}^{(K)}$ and change in η are not proportional, albeit they are correlated.

Comparing sub-shell occupation numbers OC1 and OC2, it is seen that there is sizable change (> 0.5) in η_p and η_n of different orbits in different nuclei. In the $0\nu\beta^-\beta^-$ decay of ^{94,96} Zr, the reduction in $\overline{M}^{(K)}$ is mostly related to the decrease (increase) in occupancy of $0h_{11/2}^{\pi}$ and $0g_{7/2}^{\nu}$ $(1d^{\nu})$ orbits. Here, π and ν refer to proton and neutron, respectively. The increase (decrease) in occupation numbers of $0g_{9/2}^{\pi}$ $(1p_{1/2}^{\pi}$ and $0\,h_{11/2}^{\pi})$ and $0g_{7/2}^{\nu}$, $0h_{11/2}^{\nu}$ $(1d^{\nu})$ orbits seems to be relevant for reducing $\overline{M}^{(K)}$ of ^{100}Mo. The change in η of 1 d^{π} $(1d^{\nu}, 0g_{7/2}^{\nu}$, and $0\,h_{11/2}^{\nu})$ orbit and reduction in $\overline{M}^{(K)}$ of ^{110}Pd are correlated. In the $\beta^-\beta^-$ decay of $^{!28,130}$ Te, the reduced magnitude of $\overline{M}^{(K)}$ is mostly due to the change in occupancy of $2s_{1/2}^{\nu}$, $1d^{\nu}$, $0\ g_{7/2}^{\nu}$, and $0h_{11/2}^{\nu}$ orbits. The increase (decrease) in occupation numbers of $0g_{7/2}^{\pi}$ and $0\ h_{11/2}^{\pi}$ $(1d^{\pi})$ as well as $0h_{9/2}^{\nu}$, $(1f_{7/2}^{\nu})$ orbits are related to reduction in $\overline{M}^{(K)}$ of ^{150}Nd. In general, the magnitude of $M^{(K)}$ is extremely sensitive to sub-shell occupancies of spin-orbit partner orbits in general and specifically to $1d, 0g_{7/2}$ and $0\,h_{11/2}$ orbits in the present work. Hence, the reproduction of experimental occupation numbers can be one of the criteria to test the reliability of NTMEs.

Table 8 Error correlation symmetric matrix $\rho_{XY}^{(K)}$ ($K = 0\nu$ and $0N$) for ^{130}Te, ^{94,96}Zr, ^{100}Mo, ^{110}Pd, ^{128}Te, and ^{150}Nd isotopes due to light and heavy neutrino exchange

Nucleus	^{130}Te	^{94}Zr	^{96}Zr	^{100}Mo	^{110}Pd	^{128}Te	^{150}Nd
	Light Neutrino Exchange						
^{130}Te	1.000						
^{94}Zr	0.396	1.000					
^{96}Zr	0.821	0.723	1.000				
^{100}Mo	0.744	0.880	0.958	1.000			
^{110}Pd	0.049	0.315	0.418	0.328	1.000		
^{128}Te	0.619	0.961	0.861	0.970	0.250	1.000	
^{150}Nd	0.360	0.993	0.657	0.837	0.266	0.938	1.000
	Heavy Neutrino Exchange						
^{130}Te	1.000						
^{94}Zr	0.969	1.000					
^{96}Zr	0.993	0.983	1.000				
^{100}Mo	0.988	0.995	0.996	1.000			
^{110}Pd	0.918	0.911	0.943	0.932	1.000		
^{128}Te	0.989	0.992	0.997	0.999	0.941	1.000	
^{150}Nd	0.938	0.990	0.957	0.977	0.906	0.976	1.000

Further, the nuclear sensitivities $\xi^{(K)}$ ($K = 0\nu, 0N$) defined by Šimkovic et al. [57] as

$$\xi^{(K)} = 10^8 \sqrt{G_{01}\ yr}\left|M^{(K)}\right| \tag{13}$$

with an arbitrary normalization factor 10^8 so that the nuclear sensitivities turn out to be order of unity are also calculated. The calculated nuclear sensitivities $\xi^{(0\nu)}$ ($\xi^{(0N)}$) for light (heavy) neutrino exchange are 13.72 (4.48×10^2), 55.07 (1.84×10^3), 108.7 (3.33×10^3), 50.97 (1.56×10^3), 10.06 (3.58×10^2), 76.24 (2.47×10^3), and 96.0 (2.99×10^3) for ^{94,96}Zr, ^{100}Mo, ^{110}Pd, ^{128,130}Te, and ^{150}Nd isotopes, respectively. In Fig. 1, NTMEs $M^{(0\nu)}$ and $M^{(0N)}$ calculated in different theoretical models are presented to highlight the spread in computed NTMEs. In comparison to SM and QRPA (including its extensions) values, presently calculated NTMEs $M^{(0\nu)}$ differ by a factor of about 0.5–0.9 and 0.5–2.5, respectively. However, the difference between the calculated values of $M^{(0N)}$ turns out to be a factor of about 1.3–1.6 and 1.5–7.5 in comparison to SM and QRPA (including its extensions) results.

The error correlation matrix ρ_{XY} (X and Y are two different nuclei) defined by

$$\sigma_X^{(K)}\rho_{XY}^{(K)}\sigma_Y^{(K)} = \frac{1}{N-1}\sum_{i=1}^{N}\left[\left(M_i^{(K)}(X) - \overline{M}^{(K)}(X)\right)\times\left(M_i^{(K)}(Y) - \overline{M}^{(K)}(Y)\right)\right] \tag{14}$$

is calculated to obtain additional information on the role of different ingredients, which contribute to uncertainties associated with the NTMEs.

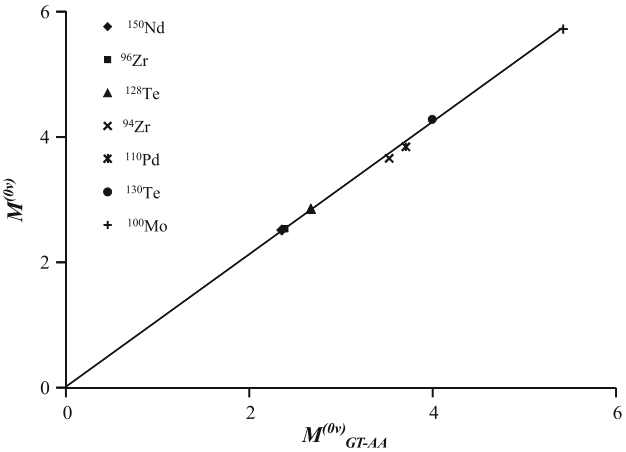

Fig. 2 Correlation between $M^{(0\nu)}$ and $M^{(0\nu)}_{GT-AA}$

In Table 8, the symmetric error correlation matrix $\rho_{XY}^{(0\nu)}$ and $\rho_{XY}^{(0N)}$ of $M^{(0\nu)}$ and $M^{(0N)}$ due to light and heavy neutrino exchange, respectively, for the set of nuclei ^{130}Te, ^{94,96}Zr, ^{100}Mo, ^{110}Pd, ^{128}Te, and ^{150}Nd are presented. In the case of light neutrino exchange, it is observed that but for ^{110}Pd and partly ^{150} Nd nuclei the set of NTMEs $M^{(0\nu)}$ are highly correlated. The error correlation matrices $\rho_{XY}^{(0N)}$ of $M^{(0N)}$ are close to one. By constraining the input parameters of theoretical calculations employing several observed data, the correlations between different nuclei can be reduced [88]. Hence, further constraints on input parameters of PHFB model on the basis of experimental data is required to reduce the calculated correlations between the NTMEs due to light and heavy neutrino exchange.

Table 9 Effective neutrino mass $\langle m_\nu \rangle$, $\langle M_N \rangle$, and predicted half-lives $T_{1/2}^{(0\nu)}$ (for light neutrino exchange at $\langle m_\nu \rangle$= 50meV) for the $0\nu\beta^-\beta^-$ decay of ^{94,96}Zr, ^{100}Mo, ^{110}Pd, ^{128,130}Te, and ^{150}Nd isotopes

Nuclei	$T_{1/2}^{(0\nu)}$(Exp.) (years)	References	Light neutrino exchange		Heavy neutrino exchange
			$\langle m_\nu \rangle$ (eV)	$T_{1/2}^{(0\nu)}$ $(years)$	$\langle M_N \rangle$ (GeV)
^{94}Zr	1.9×10^{19}	[91]	8.08×10^{2}	4.96×10^{27}	1.93×10^{4}
^{96}Zr	9.2×10^{21}	[92]	9.67	3.44×10^{26}	1.66×10^{6}
^{100}Mo	1.1×10^{24}	[93]	0.45	8.84×10^{25}	3.27×10^{7}
^{110}Pd	6.0×10^{17}	[94]	1.29×10^{3}	4.02×10^{26}	1.13×10^{4}
^{128}Te	1.5×10^{24}	[95]	4.15	1.03×10^{28}	4.12×10^{6}
^{130}Te	1.5×10^{25}	[96]	0.17	1.80×10^{26}	8.99×10^{7}
^{150}Nd	2.0×10^{22}	[97]	3.76	1.13×10^{26}	3.97×10^{6}

Employing QRPA [70] and ISM [89,90], the relation between double Gamow-Teller (DGT) matrix element $M_{GT}^{(2\nu)}$ of $2\nu\beta^-\beta^-$ decay and $M_{GT-AA}^{(0\nu)}$ of $0\nu\beta^-\beta^-$ decay has been studied. In Ref. [70], it has been observed that NTMEs $M_{GT}^{(2\nu)}$ and $M_{GT-AA}^{(0\nu)}$ are not proportional. On the other hand, in ISM, a linear correlation between $M_{GT}^{(2\nu)}$ and $M_{GT-AA}^{(0\nu)}$ has been found. By construction, the relation

$$M_{GT-K}^{(0\nu)} = \int C_{GT-K}^{(0\nu)}(r)dr = \int C_{GT}^{(2\nu)}(r) H_{GT-K}^{(0\nu)}\left(r, \overline{A}\right) dr \quad (15)$$

where $K = AA$, AP, PP, and MM is exact. In general, NTMEs $M_{GT-AA}^{(0\nu)}$ and $M^{(0\nu)}$ calculated within PHFB approach are nearly equal and the maximum difference between them is less than 8%. As an example, $M_{GT-AA}^{(0\nu)}$ and $M^{(0\nu)}$ for $PQQ1$ parametrization and SRC2 are displayed in Fig. 2. The relation between $M_{GT}^{(2\nu)}$ and $M_{GT-AA}^{(0\nu)}$ is made explicit by plotting the radial distributions of $C_{GT}^{(2\nu)}(r)$, $H_{GT-AA}^{(0\nu)}(r)$, and $C_{GT-AA}^{(0\nu)}(r)$ in Figs. 3 and 4, respectively.

As the radial distribution of $H_{GT-AA}^{(0\nu)}$ is not a constant, NTMEs $M_{GT}^{(2\nu)}$ and $M_{GT-AA}^{(0\nu)}$ are in general not proportional as observed in Ref. [70].

In Fig. 5, a linear best fit of $M_{GT}^{(2\nu)}$ vs. $M_{GT-AA}^{(0\nu)}$ is displayed for presently considered nuclei. The correlation coefficient given by

$$r = \frac{\sum_{i=1}^{N}\left(M_i^{(2\nu)} - \overline{M}^{(2\nu)}\right)\left(M_i^{(0\nu)} - \overline{M}^{(0\nu)}\right)}{\sqrt{\sum_{i=1}^{N}\left(M_i^{(2\nu)} - \overline{M}^{(2\nu)}\right)^2 \sum_{i=1}^{N}\left(M_i^{(0\nu)} - \overline{M}^{(0\nu)}\right)^2}} \quad (16)$$

turns out to be 0.974 for $M_{GT}^{(2\nu)}$ vs. $M_{GT-AA}^{(0\nu)}$. The correlation coefficient r for $M_{GT}^{(2\nu)}$ vs. $M_{GT-AA}^{(0\nu)}A^{-1/6}$ remains almost unchanged and equals to 0.970. Hence, the NTMEs $M_{GT}^{(2\nu)}$ and $M_{GT-AA}^{(0\nu)}$ are linearly correlated as observed in Ref. [89]. The effect of large configuration mixing as implemented in ISM and EDF on linear correlation between $M_{GT}^{(2\nu)}$ and $M_{GT-AA}^{(0\nu)}$ needs to be investigated, which is beyond the scope of the present work.

The limits on the effective mass of light Majorana neutrino $\langle m_\nu \rangle$ as well as heavy Majorana neutrino $\langle M_N \rangle$ are extracted from the most recent observed limits on half-lives $T_{1/2}^{0\nu}$ of $0\nu\beta^-\beta^-$ decay using the average NTMEs $\overline{M}^{(K)}$ $(K = 0\nu, 0N)$ and are presented in Table 9 along with the predicted half-lives for $\langle m_\nu \rangle = 50$ meV. We use the phase space factors G_{01} calculated by Stoica and Mirea [62] and rescale them with $g_A = 1.2701$. However, the G_{01} of ^{94}Zr isotope is not available. We calculate G_{01} for ^{94}Zr isotope without screening correction and the calculated value is 1.566×10^{-15} at $g_A = 1.2701$. The extracted upper (lower) limits on $\langle m_\nu \rangle$ ($\langle M_N \rangle$) for ^{100}Mo and ^{130} Te nuclei are 0.45 eV (3.27×10^7 GeV) and 0.17 eV (8.99×10^7 GeV), respectively.

4 Conclusions

To summarize, we have calculated the sub-shell occupation numbers, yrast spectra, and deformation parameters β_2 of ^{94,96}Zr, ^{94,96,100}Mo, ^{100}Ru, ^{110}Pd, ^{110}Cd, ^{128,130}Te, ^{128,130}Xe, ^{150}Nd, and ^{150}Sm isotopes. It has been observed that the reproduction of experimental occupation numbers plays a crucial role in improving the reliability of wave functions and hence, in the calculation of NTMEs. The overall agreement between the calculated and observed spectroscopic properties suggests that the PHFB wave functions for all four parametrizations, namely $PQQ1$, $PQQHH1$, $PQQ2$, and $PQQHH2$ are quite reliable. In closure approximation, we have also estimated NTMEs $M_{2\nu}$ of ^{94,96}Zr, ^{100}Mo, ^{110}Pd, ^{128,130}Te, and ^{150}Nd isotopes for the $2\nu\beta^-\beta^-$ decay for $0^+ \rightarrow 0^+$ transition.

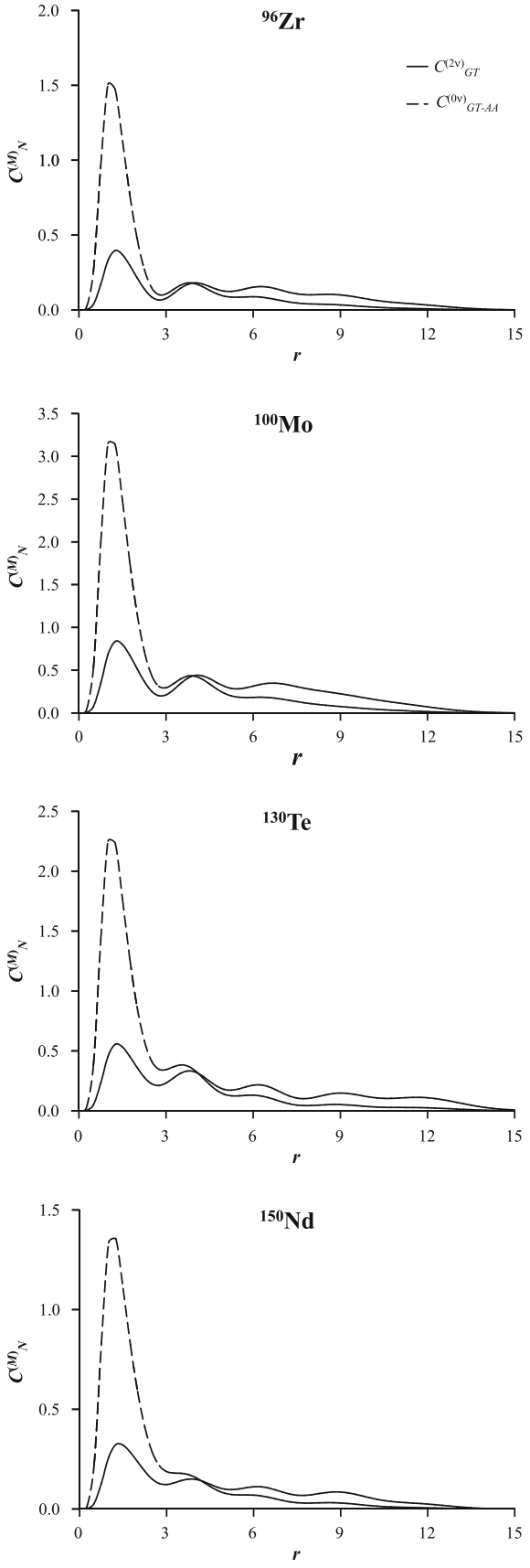

Fig. 3 Radial distributions of $C^{(2\nu)}_{GT}(r)$, and $C^{(0\nu)}_{GT-AA}(r)$ for ^{96}Zr, ^{100}Mo, ^{130}Te, and ^{150}Nd nuclei. Here M denotes 2ν, 0ν and N denotes *GT, GT-AA*

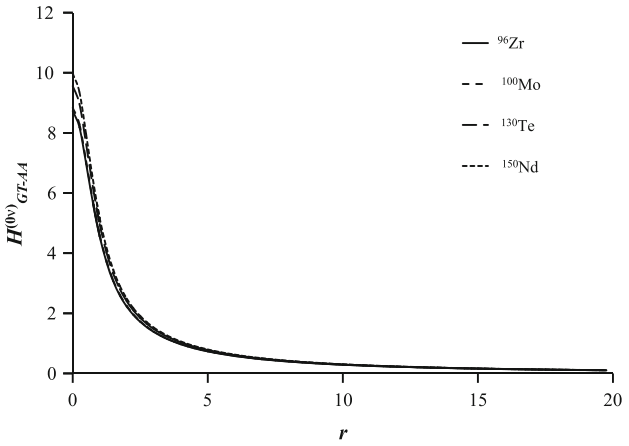

Fig. 4 Radial distribution of $H^{(0\nu)}_{GT-AA}(r)$ for ^{96}Zr, ^{100}Mo, ^{130}Te, and ^{150}Nd nuclei

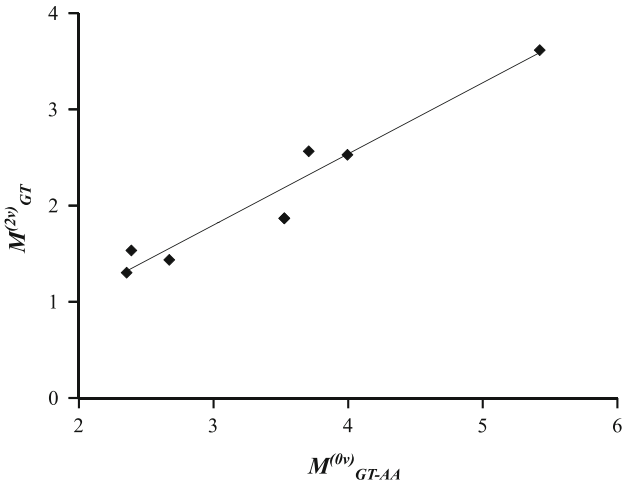

Fig. 5 Correlation between $M^{(2\nu)}_{GT}$ and $M^{(0\nu)}_{GT-AA}$

In case of $0\nu\beta^-\beta^-$ decay, it is observed that the closure approximation is quite valid as expected. The effect due to FNS is about 12 and 33% for light and heavy neutrino exchange, respectively. With the consideration of the SRCs, the NTMEs $M^{(0\nu)}$ $\left(M^{(0N)}\right)$ are in addition reduced by approximately 17% (68%), 2.0% (42%), and 3% (20%) for SRC1, SRC2, and SRC3, respectively. The effect due to deformation quantified by $D^{(K)}$ $(K = 0\nu, 0N)$ is about 2–9. It has been observed that NTMEs $\overline{M}^{(K)}$ calculated with wave functions having adjusted occupation numbers are in general of reduced magnitudes in comparison to those calculated with wave functions having unadjusted occupation numbers. Further, the relation between DGT matrix element $M^{(2\nu)}_{GT}$ and $M^{(0\nu)}_{GT-AA}$ has been explored. A linear correlation with correlation coefficient $r = 0.974$ between NTMEs $M^{(2\nu)}_{GT}$ and $M^{(0\nu)}_{GT-AA}$ is observed. Limits on the effective neutrino mass $\langle m_\nu \rangle$ and $\langle M_N \rangle$ have been extracted from the available limits on experimental half-lives $T^{0\nu}_{1/2}$ using average NTMEs

$\overline{M}^{(K)}(K = 0\nu, 0N)$ calculated within the PHFB approach. The extracted limits on $\langle m_\nu \rangle$ and $\langle M_N \rangle$ for ^{130} Te nuclei are equal to 0.17 eV and 8.99×10^7 GeV, respectively.

Acknowledgements This work is partially supported by DAE-BRNS, India vide sanction no. 58/14/08/2020-BRNS.

Data Availability Statement This manuscript has no associated data or the data will not be deposited. [Authors' comment: All the relevant and concerned data has been provided in the manuscript.]

References

1. S. Dell'Oro, S. Marcocci, M. Viel, F. Vissani, Adv. High Energy Phys. **2016**, 2162659 (2016)
2. A.S. Barabash, Int. J. Mod. Phys. A **33**, 1843001 (2018)
3. J.D. Vergados, H. Ejiri, F. Šimkovic, Int. J. Mod. Phys. E **25**, 1630007 (2016)
4. J.D. Vergados, H. Ejiri, F. Šimkovic, Rep. Prog. Phys. **75**, 106301 (2012)
5. J. Engel, J. Menéndez, Rep. Prog. Phys. **80**, 046301 (2017)
6. P. Vogel, M.R. Zirnbauer, Phys. Rev. Lett. **57**, 3148 (1986)
7. O. Civitarese, A. Faessler, T. Tomoda, Phys. Lett. B **194**, 11 (1987)
8. J. Suhonen, O. Civitarese, Phys. Rep. **300**, 123 (1998)
9. A. Faessler, F. Šimkovic, J. Phys. G **24**, 2139 (1998)
10. F. Šimkovic, V. Rodin, A. Faessler, P. Vogel, Phys. Rev. C **87**, 045501 (2013)
11. E. Caurier, F. Nowacki, A. Poves, Eur. Phys. J. A **36**, 195 (2008)
12. E. Caurier, J. Menéndez, F. Nowacki, A. Poves, Phys. Rev. Lett. **100**, 052503 (2008)
13. E. Caurier, F. Nowacki, A. Poves, J. Retamosa, Nucl. Phys. A **654**, 973c (1999)
14. E. Caurier, F. Nowacki, A. Poves, J. Retamosa, Phys. Rev. Lett. **77**, 1954 (1996)
15. J. Menéndez, A. Poves, E. Caurier, F. Nowacki, Nucl. Phys. A **818**, 139 (2009)
16. B.A. Brown, M. Horoi, R.A. Sen'kov, Phys. Rev. Lett. **113**, 262501 (2014)
17. M. Horoi, B.A. Brown, Phys. Rev. Lett. **110**, 222502 (2013)
18. M. Horoi, S. Stoica, Phys. Rev. C **81**, 024321 (2010)
19. R.A. Sen'kov, M. Horoi, Phys. Rev. C **93**, 044334 (2016)
20. B.A. Brown, D.L. Fang, M. Horoi, Phys. Rev. C **92**, 041301(R) (2015)
21. A. Neacsu, M. Horoi, Phys. Rev. C **91**, 024309 (2015)
22. R.A. Sen'kov, M. Horoi, Phys. Rev. C **90**, 051301(R) (2014)
23. R.A. Sen'kov, M. Horoi, B.A. Brown, Phys. Rev. C **89**, 054304 (2014)
24. E. Caurier, G. Martinz-Pinedo, F. Nowacki, A. Poves, A.P. Zucker, Rev. Mod. Phys. **77**, 425 (2005)
25. A. Poves, J. Phys. G Nucl. Part. Phys. **44**, 084002 (2017)
26. A. Faessler, V. Rodin, F. Šimkovic, J. Phys. G Nucl. Part. Phys. **39**, 124006 (2012)
27. D.L. Fang, A. Faessler, V. Rodin, F. Šimkovic, Phys. Rev. C **83**, 034320 (2011)
28. D.L. Fang, A. Faessler, V. Rodin, F. Šimkovic, Phys. Rev. C **82**, 051301(R) (2010)
29. M.T. Mustonen, J. Engel, Phys. Rev. C **87**, 064302 (2013)
30. D.L. Fang, A. Faessler, F. Šimkovic, Phys. Rev. C **97**, 045503 (2018)
31. P.K. Rath, R. Chandra, K. Chaturvedi, P.K. Raina, J.G. Hirsch, Phys. Rev. C **82**, 064310 (2010)
32. P.K. Rath, R. Chandra, K. Chaturvedi, P. Lohani, P.K. Raina, J.G. Hirsch, Phys. Rev. C **88**, 064322 (2013)
33. P.K. Rath, R. Chandra, P.K. Raina, K. Chaturvedi, J.G. Hirsch, Phys. Rev. C **85**, 014308 (2012)
34. P.K. Rath, R. Chandra, K. Chaturvedi, P. Lohani, P.K. Raina, Phys. Rev. C **93**, 024314 (2016)
35. T.R. Rodríguez, G. Martínez-Pinedo, Phys. Rev. Lett. **105**, 252503 (2010)
36. J.M. Yao, L.S. Song, K. Hagino, P. Ring, J. Meng, Phys. Rev. C **91**, 024316 (2015)
37. L.S. Song, J.M. Yao, P. Ring, J. Meng, Phys. Rev. C **95**, 024305 (2017)
38. J. Barea, J. Kotila, F. Iachello, Phys. Rev. C **87**, 014315 (2013)
39. F. Iachello, J. Barea, J. Kotila, AIP Conf. Proc. **1417**, 62 (2011)
40. F. Iachello, J. Barea, Nucl. Phys. B Proc. Suppl. **217**, 5 (2011)
41. J. Barea, F. Iachello, Phys. Rev. C **79**, 044301 (2009)
42. N. Yosida, F. Iachello, Prog. Theor. Exp. Phys. **2013**, 043D01 (2013)
43. J. Barea, J. Kotila, F. Iachello, Phys. Rev. C **91**, 034304 (2015)
44. G.A. Miller, J.E. Spencer, Ann. Phys. (NY) **100**, 562 (1976)
45. M. Kortelainen, J. Suhonen, Phys. Rev. C **76**, 024315 (2007)
46. M. Kortelainen, O. Civitarese, J. Suhonen, J. Toivanen, Phys. Lett. B **647**, 128 (2007)
47. F. Šimkovic, A. Faessler, H. Muther, V. Rodin, M. Stauf, Phys. Rev. C **79**, 055501 (2009)
48. J. Menéndez, D. Gazit, A. Schwenk, Phys. Rev. Lett. **107**, 062501 (2011)
49. J. Suhonen, O. Civitarese, Phys. Lett. B **725**, 153 (2013)
50. J. Engel, F. Šimkovic, P. Vogel, Phys. Rev. C **89**, 064308 (2014)
51. S.K. Khosa, P.N. Tripathi, S.K. Sharma, Phys. Lett. B **119**, 257 (1982)
52. J.D. Vergados, T.T.S. Kuo, Phys. Lett. B **35**, 93 (1971)
53. P. Federman, S. Pittel, Phys. Lett. B **77**, 29 (1978)
54. S.J. Freeman et al., Phys. Rev. C **96**, 054325 (2017)
55. B.P. Kay et al., Phys. Rev. C **87**, 011302 (2013)
56. J. Blomqvist, S. Wahlborn, Ark. Fys. **16/46**, 545 (1960)
57. F. Šimkovic, G. Pantis, J.D. Vergados, A. Faessler, Phys. Rev. C **60**, 055502 (1999)
58. J.D. Vergados, Phys. Rep. **361**, 1 (2002)
59. M. Blenow, E.F. Martinez, J.L. Pavon, J. Menéndez, JHEP07, **096** (2010)
60. F. Šimkovic, D. Štefánik, R. Dvornický, Front. Phys. **5**, 57 (2017)
61. J. Kotila, F. Iachello, Phys. Rev. C **85**, 034316 (2012)
62. S. Stoica, M. Mirea, Phys. Rev. C **88**, 037303 (2013)
63. D. Stefanik, R. Dvornicky, F. Šimkovic, P. Vogel, Phys. Rev. C **92**, 055502 (2015)
64. R. Chandra, K. Chaturvedi, P.K. Rath, P.K. Raina, J.G. Hirsch, Europhys. Lett. **86**, 32001 (2009)
65. N. Hinohara, J. Engel, Phys. Rev. C **90**, 031301(R) (2014)
66. P.J. Brussaard, P.W.M. Glaudemans, *Shell-Model Applications in Nuclear Spectroscopy* (North-Holland, Amsterdam, 1977)
67. B.H. Brandow, Rev. Mod. Phys. **39**, 771 (1967)
68. M. Hjorth-Jensen, T.T.S. Kuo, E. Osnes, Phys. Rep. **261**, 125 (1995)
69. A. Bohr, B.R. Mottelson, *Nuclear Structure*, vol. I (World Scientific, Singapore, 1998)
70. F. Šimkovic, R. Hodak, A. Faessler, P. Vogel, Phys. Rev. C **83**, 015502 (2011)
71. Pekka Pirinen, Jouni Suhonen, Phys. Rev. C **91**, 054309 (2015)
72. E. Caurier, F. Nowacki, A. Poves, Phys. Lett. B **711**, 62 (2012)
73. E. Caurier, A. Poves, A.P. Zuker, Phys. Lett. B **252**, 13 (1990)
74. E.A. Coello Perez, J. Menéndez, A. Swenk, Phys. Lett. B **797**, 134885 (2019)
75. L. Coraggio, L. De Angelis, T. Fukui, A. Gargano, N. Itaco, F. Nowacki, Phys. Rev. C **100**, 014316 (2019)
76. A.S. Barabash, Universe **6**, 159 (2020)
77. W.C. Haxton, G.J. Stephenson Jr., Prog. Part. Nucl. Phys. **12**, 409 (1984)

78. S. Raman, C.W. Nestor Jr., P. Tikkanen, At. Data Nucl. Data Tables **78**, 1 (2001)
79. S. Raman, C.H. Malarkey, W.T. Milner, C.W. Nestor Jr., P.H. Stelson, At. Data Nucl. Data Tables **36**, 1 (1987)
80. K. Chaturvedi, R. Chandra, P.K. Rath, P.K. Raina, J.G. Hirsch, Phys. Rev. C **78**, 054302 (2008)
81. J. Beringer et al. [Particle Data Group], Phys. Rev. D **86**, 010001 (2012)
82. R.A. Sen'kov, M. Horoi, Phys. Rev. C **90**, 051301(R) (2014)
83. J. Menéndez, J. Phys. G Nucl. Part. Phys. **45**, 014003 (2018)
84. M. Horoi, J. Phys. Conf. Ser. **966**, 012009 (2018)
85. J. Hyvarinen, J. Suhonen, Phys. Rev. C **91**, 024613 (2015)
86. N.L. Vaquero, T.R. Rodríguez, J.L. Egido, Phys. Rev. Lett. **111**, 142501 (2013)
87. P.K. Rath, A. Kumar, R. Chandra, R. Gautam, P.K. Raina, B.M. Dixit, Int. J. Mod. Phys. E **28**, 1950096 (2019)
88. A. Faessler, G.L. Fogli, E. Lisi, V. Rodin, A.M. Rotunno, F. Šimkovic, Phys. Rev. D **79**, 053001 (2009)
89. N. Shimizu, J. Menéndez, K. Yako, Phys. Rev. Lett. **120**, 142502 (2018)
90. C. Brase, J. Menéndez, E.A. Coello Perez, A. Swenk. arXiv:210811805v1 [nucl-th]
91. R. Arnold et al., Nucl. Phys. A **658**, 299 (1999)
92. A.S. Barabash, V.B. Brudanin, Phys. At. Nucl. **74**, 312 (2011)
93. R. Arnold et al., Phys. Rev. D **92**, 072011 (2015)
94. R.G. Winter, Phys. Rev. **85**, 687 (1952)
95. A.S. Barabash, Nucl. Phys. A **935**, 52 (2015)
96. C. Alduino et al., Phys. Rev. Lett. **120**, 132501 (2018)
97. R. Arnold et al., Phys. Rev. D **94**, 072003 (2016)